IDEAS EN CIENCIAS DE LA INGENIERÍA

Enfoque experimental óptico para la emulación del comportamiento direccional del beamforming de radiofrecuencia para el estudio de la captación inalámbrica de energía

An optical experimental approach for emulating the directional behavior of radio-frequency beamforming for wireless energy harvesting studies

E. Gutiérrez[1], C. Castorena[2] *, J. A. De Rus[2], S. Roger[2], C. Botella-Mascarell[2]
(*carlos.castorena@uv.es)

Recibido: 16 de septiembre de 2026 Aceptado: 13 de octubre de 2026

Resumen

La generación de haces de radiofrecuencia mediante beamforming permite dirigir la potencia transmitida hacia determinadas regiones del espacio, lo que resulta de interés en aplicaciones de captación inalámbrica de energía y gestión de la energía disponible en dispositivos. En estos sistemas, conocer cómo varía la potencia recibida según la posición y orientación del receptor es relevante para estudiar las condiciones de disponibilidad energética y las decisiones asociadas a su administración. Aunque este comportamiento puede analizarse mediante modelos matemáticos y simulaciones numéricas, su estudio experimental mediante sistemas de radiofrecuencia requiere hardware específico para generar, controlar y medir los haces, lo que puede resultar costoso cuando se necesitan múltiples condiciones de operación. En este trabajo se propone un enfoque experimental óptico para emular la potencia de radiofrecuencia que estaría disponible en diferentes posiciones y orientaciones respecto a un haz generado mediante beamforming. El sistema utiliza una fuente luminosa para generar un haz dirigido y un receptor óptico para registrar su distribución angular. La propuesta no busca reproducir la transferencia de energía ni la física electromagnética del haz de radiofrecuencia, sino proporcionar una representación experimental de su potencia recibida equivalente. Para ello, las lecturas del receptor óptico se relacionan mediante una función empírica con la potencia proporcionada por un modelo matemático de radiofrecuencia. Los resultados muestran que el sistema óptico permite

[1]Tecnológico Nacional de México, Campus Toluca, Toluca, Estado de México, México.
[2]Universitat de València, Departamento de Informática, València, España.

https://doi.org/10.36677/rici.v4i3.29503 ISSN: 2992-7447 Noviembre 2026 - Febrero 2027 págs. 89- 105

representar experimentalmente determinadas características direccionales del modelo de referencia de radiofrecuencia, particularmente la dirección del máximo y la magnitud de la potencia recibida, bajo las condiciones evaluadas.

Palabras clave: haces de radiofrecuencia, distribución angular, captación inalámbrica de energía

Abstract

The generation of radio-frequency beams through beamforming enables transmitted power to be directed toward specific regions of space, which is of interest in wireless energy harvesting and in managing the energy available to devices. In these systems, understanding how the received power varies with the position and orientation of the receiver is relevant for studying energy availability conditions and the decisions associated with energy management. Although this behavior can be analyzed using mathematical models and numerical simulations, its experimental study using radio-frequency systems requires specific hardware to generate, control, and measure the beams, which can become costly when multiple operating conditions need to be investigated. This work proposes an optical experimental approach to emulate the radio-frequency power that would be available at different positions and orientations with respect to a beam generated through beamforming. The system uses a light source to generate a directed beam and an optical receiver to record its angular distribution. The proposed approach does not seek to reproduce energy transfer or the electromagnetic physics of the radio-frequency beam, but rather to provide an experimental representation of its equivalent received power. To this end, the optical receiver readings are related through an empirical function to the power provided by a mathematical radio-frequency model. The approach is evaluated by comparing the amplitude, angular position, and angular width of the optical and radio-frequency distributions. The results show that the optical system can experimentally represent selected directional characteristics of the RF reference model, particularly the peak direction and received-power magnitude, under the evaluated conditions.

Keywords: *radio-frequency beams, angular distribution, wireless energy harvesting*

Introduction

Beamforming is a fundamental technique in radio-frequency (RF) systems for controlling the spatial distribution of transmitted energy. By appropriately controlling the signals radiated by multiple antenna elements, transmitted power can be concentrated toward selected spatial or angular regions [1]. This capability is used in communications, localization [2, 3], sensing [4], wireless power transfer [5], and RF energy harvesting [6, 7].

In RF energy harvesting, the power available at a receiving device depends not only on the transmitted

power and propagation conditions, but also on the spatial distribution of the transmitted energy [8]. Beam direction, spatial alignment, and beam width can therefore affect the energy collected by a receiver [9], particularly when multiple receivers or changing device positions are considered. Characterizing the spatial behavior of directional beams is thus relevant for understanding the power available to energy-harvesting devices under different physical conditions.

Beamforming behavior can be studied using mathematical models and numerical simulations [10, 11], which allow different antenna configurations, transmission powers, distances, and beam directions to be evaluated without a physical implementation. However, experimental conditions may introduce positioning errors, angular misalignment, measurement noise, channel uncertainty, and hardware nonidealities that are not fully represented by idealized models. Direct experimental characterization with RF hardware can capture these effects, but requires systems for generating, controlling, and measuring directional transmission [12, 13]. Such implementations may involve antenna arrays, RF sources, phase or amplitude control, power amplifiers, receivers or rectennas, and measurement instrumentation, making extensive measurement campaigns demanding.

To provide a lower-complexity experimental alternative, this work proposes an optical approach for studying selected observable characteristics of an RF beam generated through beamforming. A directional light source and an optical receiver are used to measure an angular response that experimentally represents beam direction, angular position, and angular width. The optical measurements are related to a mathematical RF model through an empirical correspondence function, allowing the measured optical response to be expressed as an equivalent RF received-power value. Because the measurements are obtained from a physical setup, experimental effects such as positioning errors, angular misalignment, measurement noise, and other nonidealities can also be incorporated into the evaluation.

Optical technologies have previously been investigated for directional wireless energy transmission, beam steering, and beam shaping. Optical wireless power transfer systems with dynamic beam steering have been demonstrated [14], as have approaches for controlling optical beam shape for wireless power transmission [15]. Optical technologies have also been incorporated into RF wireless power transfer systems for target detection and positioning, enabling RF transmission to adapt to receiver location [16].

The role of the optical system proposed here is fundamentally different. The optical beam is neither used as an energy carrier, nor to generate or control the RF signal, nor to locate the receiver. Instead, it serves as an experimental analogue of selected observable characteristics of a directional RF beam. Its measured angular distribution is empirically related to RF received power using a mathematical RF model as reference, without assuming electromagnetic or physical equivalence between the two systems. The main contribution is therefore the experimental demonstration and evaluation of this optical analogue as a lower-

https://doi.org/10.36677/rici.v4i3.29503 ISSN: 2992-7447 Noviembre 2026 - Febrero 2027 págs. 89- 105

complexity means of studying selected directional characteristics of RF beamforming, particularly the power available at receiving locations in wireless energy harvesting and energy management applications. The proposed platform also provides an accessible tool for scientific and technological education, enabling the experimental exploration of directional beam characteristics and spatial power availability without requiring specialized RF hardware.

RF Beamforming Model

The purpose of the RF model is to describe how the power available at a receiving location varies as the direction of the transmitted beam is changed. In this work, the analysis considers a two-dimensional configuration based on a uniform linear array (ULA), in which the beam can be steered within a single plane. The transmitter (TX) is represented by a ULA with N_{tx} antenna elements, while the receiver (RX) is represented by a single receiving antenna located at a distance d from the TX and at an angular position ϕ with respect to the TX. The direction toward which the transmitted beam is steered is denoted by θ. Thus, ϕ describes the position of the receiver, whereas θ describes the direction of the transmitted beam. The considered geometry and the corresponding angular received-power response are illustrated in Figure 1.

The TX operates at a carrier frequency f_c, which determines the free-space wavelength $\lambda = c/f_c$, where c denotes the speed of light in free space. The ULA is configured with an inter-element spacing of $\lambda/2$, a conventional configuration for phased-array beamforming that avoids grating lobes over the visible angular region under the ideal array model [17]. To describe how the array responds to different spatial directions, it is necessary to represent the phase relationship between the signals observed at the individual

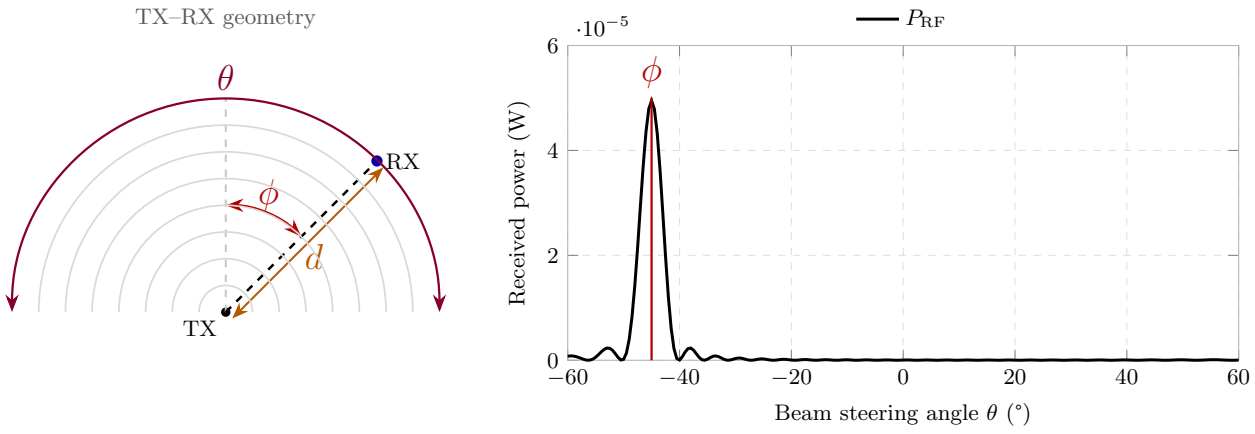


FIGURA 1. TX–RX geometry and corresponding angular received-power response for the two-dimensional ULA configuration considered in this work. The RX is located at a TX–RX distance d and angular position ϕ with respect to the TX, while θ denotes the beam steering direction. For a fixed receiver position, sweeping θ produces the angular RF received-power response P_{RF}.

antenna elements for a given direction. This directional dependence is represented by the steering vector. For a generic angular direction ψ, the normalized steering vector of the ULA is defined in Eq. (1) as follows:

$$\mathbf{a}(\psi) = \frac{1}{\sqrt{N_{tx}}} \begin{bmatrix} 1 & e^{-j\pi \sin(\psi)} & \cdots & e^{-j\pi(N_t-1)\sin(\psi)} \end{bmatrix}^T. \tag{1}$$

The angle ψ represents a generic spatial direction, while $\mathbf{a}(\psi)$ describes the phase progression across the array elements associated with that direction. The normalization ensures that $\|\mathbf{a}(\psi)\|^2 = 1$, separating the directional response from the overall transmitted-power scale. The steering vector provides a representation of the spatial response of the array for a given direction. In the considered configuration, two directions are of particular interest: the angular position of the RX, ϕ, and the beam steering direction, θ. Their spatial relationship can be quantified through the inner product between the corresponding steering vectors, presented in Eq. (2).

$$\mathbf{a}^H(\phi)\mathbf{a}(\theta). \tag{2}$$

Where $(\cdot)^H$ denotes the Hermitian transpose, i.e., the complex conjugate transpose. Thus, $\mathbf{a}^H(\phi)\mathbf{a}(\theta)$ provides a scalar measure of the spatial alignment between the RX direction ϕ and the beam steering direction θ. The magnitude of this inner product is maximized when the steering direction coincides with the RX angular position, i.e., when $\theta = \phi$. As θ is varied for a fixed ϕ, the magnitude of this term describes how strongly the transmitted beam is spatially aligned with the RX direction and therefore determines the angular variation of the received-power response. The propagation between the TX and RX is modeled as a single line-of-sight (LOS) free-space path. Its complex propagation coefficient is given by Eq. (3).

$$g(d) = \frac{\lambda}{4\pi d} e^{-j\frac{2\pi d}{\lambda}}. \tag{3}$$

Where d is the TX–RX distance. The magnitude of $g(d)$ describes the attenuation associated with free-space propagation, while its phase represents the propagation delay. This formulation follows the free-space propagation relationship underlying the Friis transmission model and its extensions to multiport and beamformed antenna systems [18]. Combining the spatial alignment of the array with the free-space propagation coefficient, the received RF power for a transmitted power P_{tx} is modeled in Eq. (4) as:

$$P_{\mathrm{RF}}(\theta, \phi, d) = P_{tx} N_{tx} \left| g(d)\mathbf{a}^H(\phi)\mathbf{a}(\theta) \right|^2. \tag{4}$$

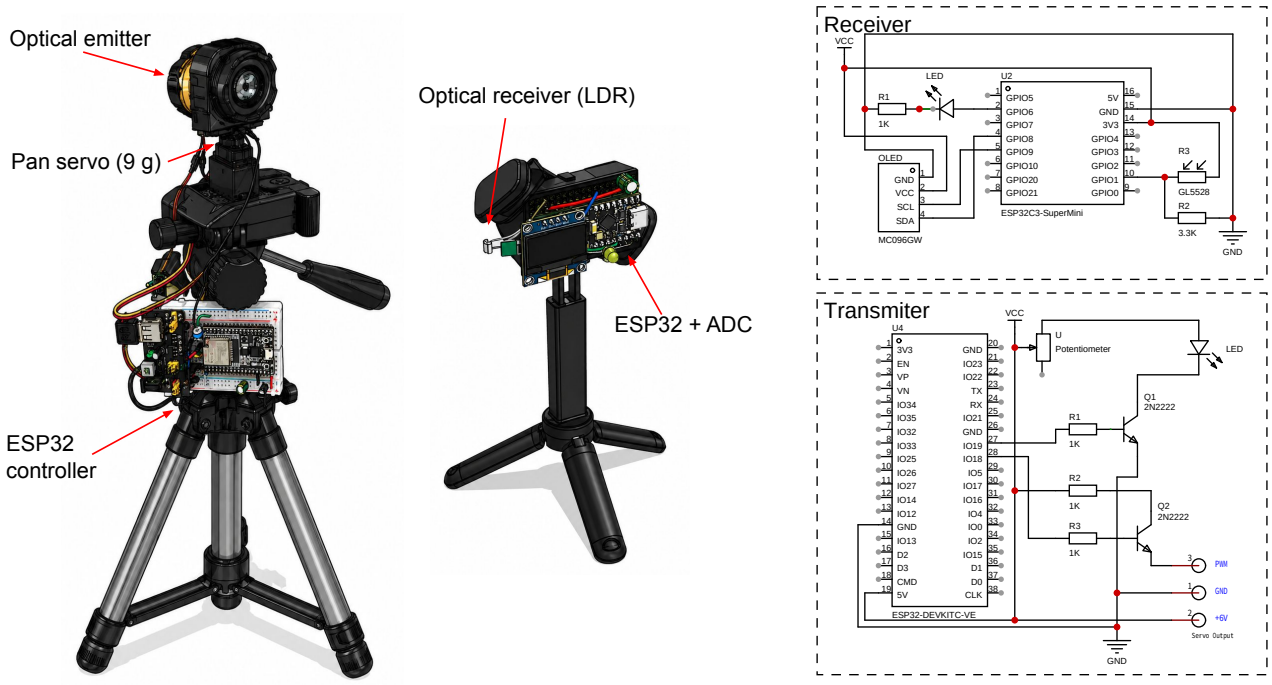
https://doi.org/10.36677/rici.v4i3.29503 ISSN: 2992-7447 Noviembre 2026 - Febrero 2027 págs. 89- 105

Here, P_{tx} denotes the transmitted power associated with each antenna element, while the factor N_{tx} accounts for the total transmitted power of the array under the adopted normalization. The expression contains two main contributions to the received-power response. The term $|g(d)|^2$ determines the distance-dependent magnitude through free-space propagation, whereas the term $|\mathbf{a}^H(\phi)\mathbf{a}(\theta)|^2$ determines the angular behavior through the spatial alignment between the RX direction and the beam steering direction. Therefore, for a fixed TX–RX distance, varying θ changes the angular response without modifying the propagation loss. Conversely, changing d modifies the received-power magnitude through the free-space propagation term. The RF reference considered in this work is an ideal ULA model under free-space LOS propagation, rather than measurements from a physical RF antenna array.

EXPERIMENTAL OPTICAL SYSTEM AND RF–OPTICAL CORRESPONDENCE

Experimental Optical Platform

The proposed experimental platform consists of an optical transmitter and an optical receiver designed to provide an experimental representation of selected observable characteristics of the angular behavior of a directional RF beam. The complete platform is shown in Figure 2, where the physical implementation is



(a) Physical implementation. (b) Electrical circuit.

FIGURA 2. Experimental optical platform used to characterize the proposed RF–optical correspondence. (a) Physical implementation of the optical transmitter and receiver. (b) Electrical circuit of the experimental platform.

presented in Figure 2(a) and the corresponding electrical circuits are shown in Figure 2(b). The platform is implemented using two ESP32-based control units: one associated with the optical transmitter and the angular positioning mechanism, and the other associated with the optical receiver and data acquisition.

The optical transmitter consists of a low-cost commercial flashlight containing three LEDs, nominally operating at $4{,}5$ V, mounted on a 9 g pan servo. The servo allows the direction of the emitted beam to be varied by changing its angular position. The flashlight incorporates a movable focusing lens that allows the beam divergence to be adjusted approximately between 5° and 15° by changing the distance between the lens and the LEDs. The optical emitter is driven through a transistor stage, and a potentiometer is included in the transmitter circuit to adjust its operating condition. The servo was controlled using angular increments of 1°, corresponding to the angular sampling step used in the experimental measurements. This increment represents the commanded angular step rather than an independently measured mechanical positioning resolution. The electrical implementation of these elements is shown in the transmitter circuit of Figure 2(b). By changing the servo position, the direction of the optical beam can be varied over a predefined angular range (θ), while the adjustable lens allows its angular width to be controlled. These two degrees of control provide an experimental means of varying the beam direction and angular width corresponding to the steering-angle and beam-width characteristics considered in the RF model.

The optical receiver consists of an LDR connected to an ESP32-C3 for analog signal acquisition. During the experiments, the receiver is placed at a prescribed TX–RX distance d and angular position ϕ with respect to the transmitter, following the geometry defined in the RF model. The LDR is incorporated into a voltage-divider circuit with a $3{,}3$ kΩ resistor, and the resulting voltage is measured through an analog input of the ESP32-C3. The receiver circuit also includes an LED used as a local indicator and an OLED display connected through an I^2C interface for monitoring the measurement system. The physical implementation of the receiver and its corresponding electrical circuit are shown in Figure 2(a) and Figure 2(b), respectively. During an angular measurement, the receiver remains at the prescribed position (d, ϕ) while the transmitter changes the orientation of the optical emitter over the selected angular range. The receiver records the response of the LDR as an ADC value at each angular position. Consequently, the receiver provides a measurement of the optical response for a given TX–RX distance and receiver angular position rather than a direct measurement of RF power.

RF–Optical Correspondence

The optical receiver provides a measured ADC value for each experimental configuration defined by the beam steering angle θ, receiver angular position ϕ, and TX–RX distance d. This measured value is denoted as $ADC_{\theta,\phi,d}$. The purpose of the RF–optical correspondence is to establish an empirical relationship between the optical measurements and the RF received power $P_{\mathrm{RF}}(\theta, \phi, d)$ obtained from the mathematical model in Eq. (4), considering the same experimental configuration (θ, ϕ, d). The corresponding quantity

https://doi.org/10.36677/rici.v4i3.29503 ISSN: 2992-7447 Noviembre 2026 - Febrero 2027 págs. 89- 105

obtained from the optical measurements is later denoted as P_{OP} and represents an equivalent RF-power value expressed on the scale of the RF reference model.

The calibration measurements are acquired at three TX–RX distances, $d = 1{,}0$, $1{,}5$, and $2{,}0$ m. For the calibration configurations, the receiver is positioned at $\phi = 0°$, while the optical emitter is swept over $\theta = -20°$ to $\theta = 20°$ in $1°$ increments. The choice of $\phi = 0°$ is made to establish the RF–optical correspondence under a reference alignment condition. In the RF model, changing the relative angular alignment between the RX position ϕ and the beam steering direction θ can modify not only the amplitude of the received-power response but also its angular width and shape. The optical system considered in this work does not provide an equivalent mechanism for reproducing this dependence: the angular width of the optical beam is determined by the emitter lens and remains approximately constant as the beam is steered. Consequently, the correspondence is established for the reference condition $\phi = 0°$, where the optical system can be adjusted to reproduce the angular width of the corresponding $N_{tx} = 32$ antenna RF response. The RF frequency is likewise fixed because the spatial response of the array and the propagation characteristics depend on the carrier frequency. In this work, the RF reference model is therefore limited to $f_c = 2{,}4$ GHz, and the optical beam is adjusted to represent the directional response associated with this configuration. The transmitter and receiver are positioned in the same horizontal plane using a laser level to reduce geometric misalignment during the measurements.

The measured ADC response is affected by measurement noise and experimental variations. To reduce the influence of individual deviations when estimating the quantities required for calibration, the measured values $ADC_{\theta,\phi,d}$ obtained during each angular sweep are fitted to a Gaussian distribution with an offset, following Eq. (5).

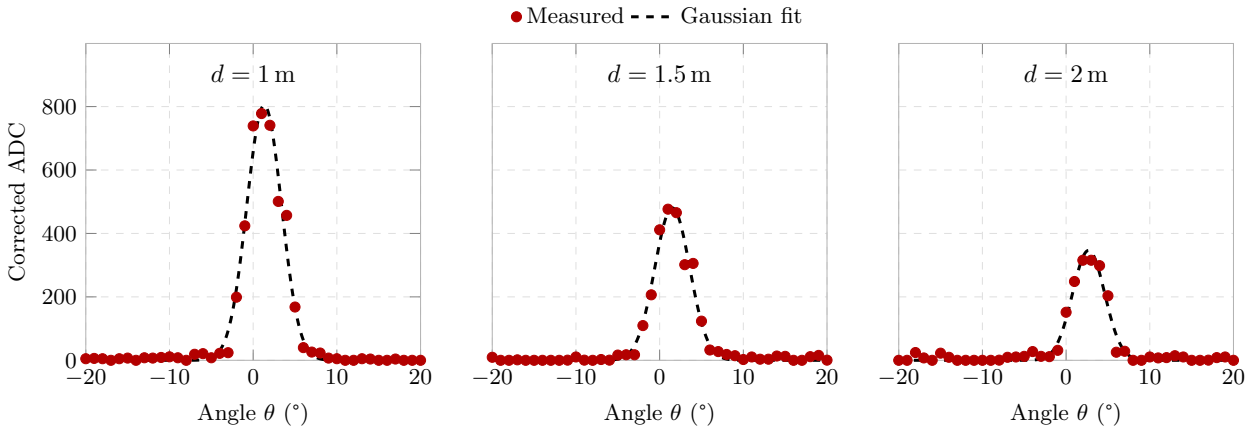


FIGURA 3. Measured corrected ADC response and Gaussian fit for the three TX–RX distances considered.

$$ADC^{\text{fit}}_{\phi,d}(\theta) = B_{\phi,d} + A_{\phi,d} \exp\left[-\frac{1}{2}\left(\frac{\theta - \mu_{\phi,d}}{\sigma_{\phi,d}}\right)^2\right]. \tag{5}$$

Where $B_{\phi,d}$ represents the estimated measurement floor, $A_{\phi,d}$ is the amplitude of the directional response above this floor, $\mu_{\phi,d}$ is the angular position of the maximum response, and $\sigma_{\phi,d}$ represents its angular spread. Figure 3 shows the measured responses and their corresponding Gaussian fits for the three TX–RX distances considered during calibration. The fitted distributions provide a representative description of the measured angular response while reducing the influence of individual deviations in the ADC measurements.

The calibration is based on the maximum amplitude $A_{\phi,d}$ obtained from each fitted angular distribution. For each experimental condition, the corresponding transmitted power P_{tx} and TX–RX distance d are associated with the measured amplitude $A_{\phi,d}$, while the RF received power is calculated from the mathematical model in Eq. (4).

The empirical RF–optical correspondence is obtained by fitting the RF reference power to the optical response amplitude according to $P_{\text{OP}}(0, \phi, d) = \alpha P_{tx} \left[A_{\phi,d}\right]^{\beta} \approx P_{\text{RF}}(0, \phi, d)$, where α and β are empirical parameters obtained from the calibration. The transmitted power $P_t x$ is maintained as a multiplicative factor because the RF received-power model in Eq. (4) is linear with respect to $P_t x$ under the adopted formulation. Consequently, the nonlinear dependence between the optical response amplitude and the RF-power scale is represented by β.

The calibration campaign uses 20 transmitted-power levels, from $0{,}25$ to $5{,}0$ W in increments of $0{,}25$ W, for each of the three TX–RX distances, resulting in 60 calibration conditions. For each condition, the maximum amplitude $A_{\phi,d}$ obtained from the corresponding Gaussian fit is paired with the RF received power calculated using the same transmitted power and TX–RX distance.

Since the RF reference power depends on the TX–RX distance, the uncertainty associated with the distance measurement is incorporated into the calibration procedure. For each Monte Carlo realization, the nominal distance associated with each experimental configuration is perturbed according to its corresponding measurement uncertainty, and the RF received power is recalculated using the perturbed distance. The resulting RF reference values are then paired with the corresponding optical amplitudes and used to repeat the calibration.

The empirical parameters are obtained by solving the nonlinear least-squares problem presented in Eq. (6).

https://doi.org/10.36677/rici.v4i3.29503 ISSN: 2992-7447 Noviembre 2026 - Febrero 2027 págs. 89- 105

$$(\hat{\alpha}, \hat{\beta}) = \arg\min_{\alpha,\beta} \sum_{i=1}^{60} \left[P_{\mathrm{RF},i} - \alpha P_{tx,i} \left(A_{\phi_i,d_i} \right)^{\beta} \right]^2 . \tag{6}$$

Where i denotes the calibration condition. For each Monte Carlo realization, the perturbed distances are used to recalculate the 60 RF reference powers, after which the nonlinear regression is solved to obtain a corresponding pair $(\hat{\alpha}, \hat{\beta})$. Repeating this procedure produces distributions of the calibration parameters that quantify the sensitivity of the empirical correspondence to the uncertainty in the TX–RX distance. This Monte Carlo analysis focuses on transmitter–receiver distance uncertainty and does not represent a complete uncertainty budget for the experimental platform. Additional sources of variability include servo positioning, optical alignment, LDR response, ambient illumination, ADC quantization, and emitter stability.

Results and Discussion

RF–Optical Correspondence Calibration

The effect of the TX–RX distance uncertainty on the empirical correspondence parameters is shown in Figure 4. The Monte Carlo analysis produces well-defined distributions for both $\hat{\alpha}$ and $\hat{\beta}$, although their spreads are different. The distribution of $\hat{\alpha}$ exhibits a larger relative dispersion and a positive skew, whereas the distribution of $\hat{\beta}$ is more concentrated around its central value. This difference is expected because $\hat{\alpha}$ primarily determines the overall power scale of the correspondence, making it more sensitive to variations in the RF reference power caused by the TX–RX distance. In contrast, $\hat{\beta}$ characterizes the nonlinear dependence between the ADC response and the RF-power scale and is less directly affected by a common scaling variation in the reference power.

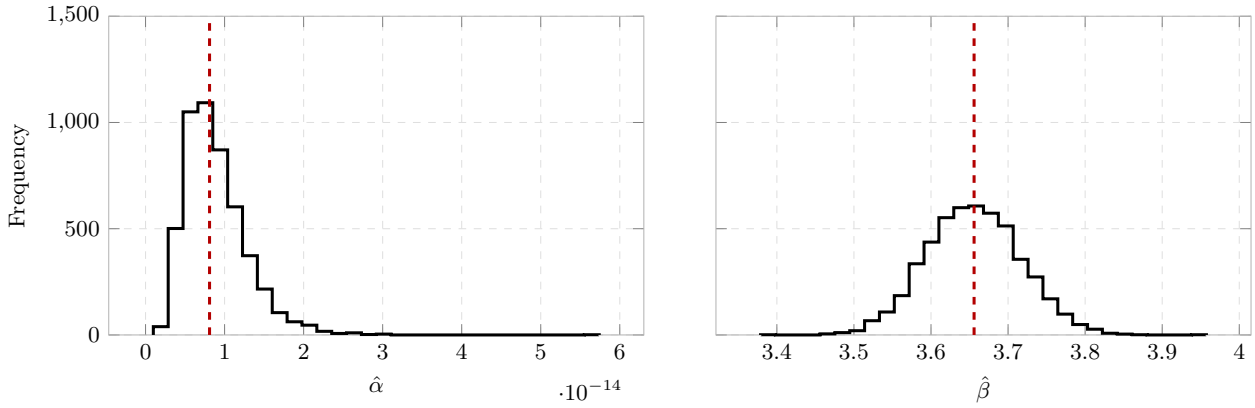


FIGURA 4. Monte Carlo distributions of the empirical RF–optical correspondence parameters. The dashed red lines indicate the median values of (a) $\hat{\alpha}$ and (b) $\hat{\beta}$.

The median values obtained from the Monte Carlo distributions are $\hat{\alpha} = 8{,}0978 \times 10^{-15}$ and $\hat{\beta} = 3{,}6559$. These values are used as the nominal parameters of the RF–optical correspondence for the subsequent analysis. The use of the median is appropriate for the present uncertainty analysis because the resulting parameter distributions, particularly that of $\hat{\alpha}$, are not perfectly symmetric. Therefore, the median provides a representative central value without requiring the distribution to be symmetric around its center.

Using these parameters, the maximum equivalent RF power obtained from the optical measurements is compared with the maximum RF received power calculated from the reference model. Figure 5 presents the resulting relationship for the 60 calibration conditions. The 20 RF transmit-power levels were introduced numerically, while the optical emitter intensity remained fixed. Thus, these levels do not represent independent optical measurements. The experimental component of the calibration lies in the variation of the transmitter–receiver distance, which produces measurable changes in the received optical response even at a fixed emitter intensity. The measurements cover the three TX–RX distances and the complete range of transmitted powers considered in the calibration. The points remain closely grouped

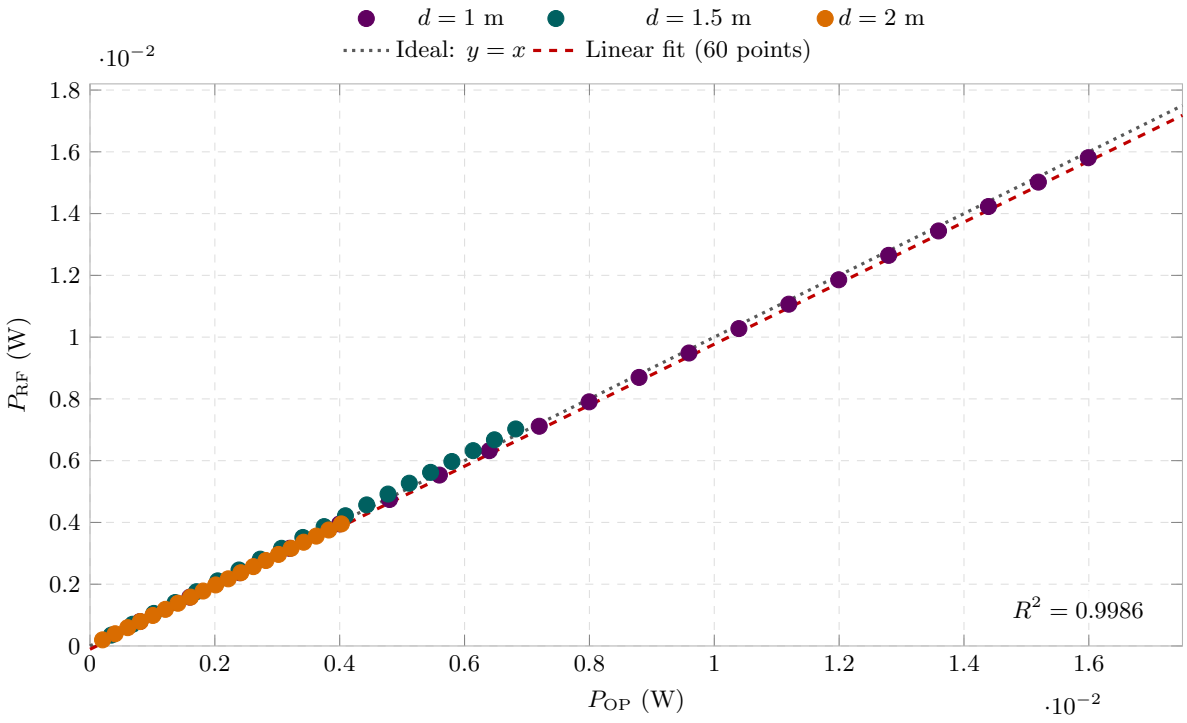


FIGURA 5. Comparison between the maximum equivalent RF received power, P_{OP}, obtained from the optical measurements and the maximum RF received power, P_{RF}, obtained from the reference model. The 60 calibration points correspond to three TX–RX distances and 20 transmitted-power levels at each distance. Point colors indicate the TX–RX distance. The dotted line represents the ideal unit-slope relationship, while the dashed red line represents the linear regression obtained from all 60 points.

https://doi.org/10.36677/rici.v4i3.29503 ISSN: 2992-7447 Noviembre 2026 - Febrero 2027 págs. 89- 105

around the identity relationship, indicating that the optical measurements can be mapped to the RF power scale over the evaluated operating range.

A linear regression of the maximum values gives a slope of $0{,}9878$, an intercept of $-1{,}0661 \times 10^{-4}$ W, and a coefficient of determination of $R^2 = 0{,}9986$. The slope is close to unity, indicating that the variation of the equivalent RF power obtained from the optical measurements follows the variation of the RF reference power with a small deviation in scale. The intercept is small compared with the maximum power values considered in the calibration, while the coefficient of determination indicates that the linear relationship accounts for almost all of the observed variation in the 60 calibration points.

The agreement between P_{OP} and P_{RF} reflects the consistency of the calibrated power mapping across the evaluated distances and numerically introduced RF transmit-power levels. The result therefore indicates that the empirical function is able to establish a consistent power-scale correspondence across the evaluated conditions. In particular, the near-unity regression slope shows that the calibrated optical response preserves the dependence of the maximum equivalent received power on the transmitted-power and distance conditions represented by the RF model.

The regression result, however, should be interpreted as a validation of the amplitude correspondence rather than as evidence of electromagnetic equivalence between the optical and RF systems. The optical receiver does not measure RF power directly; instead, the optical ADC response is transformed through the empirically calibrated function. The high value of R^2 therefore indicates the consistency of this empirical mapping with the RF reference model over the calibration conditions, rather than equivalence between the underlying physical mechanisms.

The calibration establishes the amplitude correspondence required to express the optical measurements on the RF-power scale. It does not, by itself, demonstrate that the optical system reproduces the complete directional behavior of the RF beam. This aspect requires comparison of the angular distributions, including their peak position and angular width, which is considered in the following subsection.

Experimental Validation of the Optical Approach

The results in Table 1 show that the angular position of the optical response remains close to the position predicted by the RF model for the six evaluated conditions. Except for E2, where the difference is $2{,}321°$, the absolute peak-position error remains below $1°$, with errors below $0{,}01°$ for E5 and E6. This indicates that the proposed optical representation preserves the angular location of the directional response over the evaluated range of receiver positions. The largest angular deviation was observed for configuration E2 ($2{,}321°$). This discrepancy may result from a combination of servo positioning uncertainty, mechanical alignment, and the optical beam characteristics. Since these contributions were not independently characterized, the deviation cannot be attributed to a single source.

Tabla 1. Experimental validation results for the six measurement conditions. The optical and RF peak positions are denoted by μ_{OP} and μ_{RF}, respectively. The position error is defined as $\mu_{\mathrm{OP}} - \mu_{\mathrm{RF}}$. The amplitude error and angular widths are obtained from the corresponding optical and RF power distributions.

Test	d (m)	ϕ (deg)	P_{tx} (W)	μ_{OP} (deg)	μ_{RF} (deg)	$\Delta\mu$ (deg)	E_A (%)	$\mathrm{FWHM}_{\mathrm{OP}}$ (deg)	$\mathrm{FWHM}_{\mathrm{RF}}$ (deg)
E1	1.0	-50	1	$-50{,}667$	$-49{,}997$	$-0{,}680$	$4{,}416$	$2{,}178$	$4{,}922$
E2	1.2	-35	1	$-32{,}667$	$-34{,}992$	$2{,}321$	$-5{,}016$	$2{,}178$	$3{,}841$
E3	1.4	-10	1	$-9{,}000$	$-9{,}983$	$0{,}983$	$-9{,}539$	$2{,}396$	$3{,}161$
E4	1.6	10	1	$10{,}667$	$9{,}983$	$0{,}684$	$-4{,}544$	$2{,}396$	$3{,}161$
E5	1.8	35	1	$35{,}000$	$34{,}992$	$0{,}008$	$4{,}137$	$2{,}396$	$3{,}841$
E6	2.0	50	1	$50{,}000$	$49{,}997$	$0{,}003$	$3{,}333$	$2{,}178$	$4{,}922$

The amplitude comparison presents a larger variability than the peak-position comparison. For E1–E6, the amplitude error (E_a) remains within approximately $10\,\%$. This difference should not be interpreted exclusively as an error introduced by the RF–optical correspondence. The optical measurements are affected by the experimental conditions under which each dataset is acquired, including the background optical level, measurement noise, positioning uncertainty, and other nonidealities of the experimental setup. Consequently, the amplitude discrepancy represents the combined effect of the correspondence approximation and the physical and measurement conditions present during the experiment.

This behavior is consistent with the purpose of the proposed experimental approach. Rather than attempting to reproduce an ideal RF beamforming response under controlled numerical conditions, the optical system provides a physical measurement of the directional response under the conditions present during the experiment. Variations in the measured amplitude can therefore contain information associated with environmental and experimental factors that are not explicitly represented in the ideal RF model. In this sense, the observed differences are not necessarily undesirable, since they provide an experimentally accessible representation of deviations in the power available at the receiving location.

The angular widths are characterized using the full width at half maximum (FWHM), defined as the angular separation between the two points at which the response reaches half of its maximum value. The measured optical FWHM ranges from $2{,}178^\circ$ to $2{,}396^\circ$, whereas the RF model produces values between $3{,}161^\circ$ and $4{,}922^\circ$. This difference indicates that, although the optical approach preserves the angular position of the main response, the angular spread is not reproduced with the same magnitude in all evaluated conditions. Therefore, the optical representation should be understood as an experimental analogue of selected directional characteristics rather than as a complete reproduction of the RF beam pattern.

https://doi.org/10.36677/rici.v4i3.29503 ISSN: 2992-7447 Noviembre 2026 - Febrero 2027 págs. 89- 105

Figure 6 provides a direct visualization of the agreement between the optical and RF responses. In all six cases, the main optical response is located close to the maximum of the corresponding RF distribution, despite the different receiver positions and distances. The optical curves also reproduce the localized nature of the directional response, although their angular widths differ from those predicted by the RF model. The differences in amplitude are more pronounced than the differences in angular position, particularly for conditions in which the RF reference power becomes small. These results further support the interpretation of the optical system as an experimental representation of selected observable beam characteristics rather than a physically equivalent RF system.

The experimental validation was conducted using six receiver configurations with different angular positions and transmitter–receiver distances, distinct from the reference calibration direction. The RF comparison was restricted to an ideal 32-element ULA operating at 2.4 GHz under LOS propagation. Therefore, the reported results demonstrate the feasibility of representing selected directional characteristics within the evaluated configurations, rather than establishing general applicability to arbitrary RF beamforming systems.

To facilitate the use and reproducibility of the proposed approach, a web-based application was developed for RF–optical calibration and experimental evaluation. The application allows users to upload optical measurements, estimate the empirical parameters α and β, compare new measurements with the RF reference model, and export the resulting power distributions for further analysis. The application is publicly available at https://www.uv.es/carcasla/proyectos/rf_optical_web/in

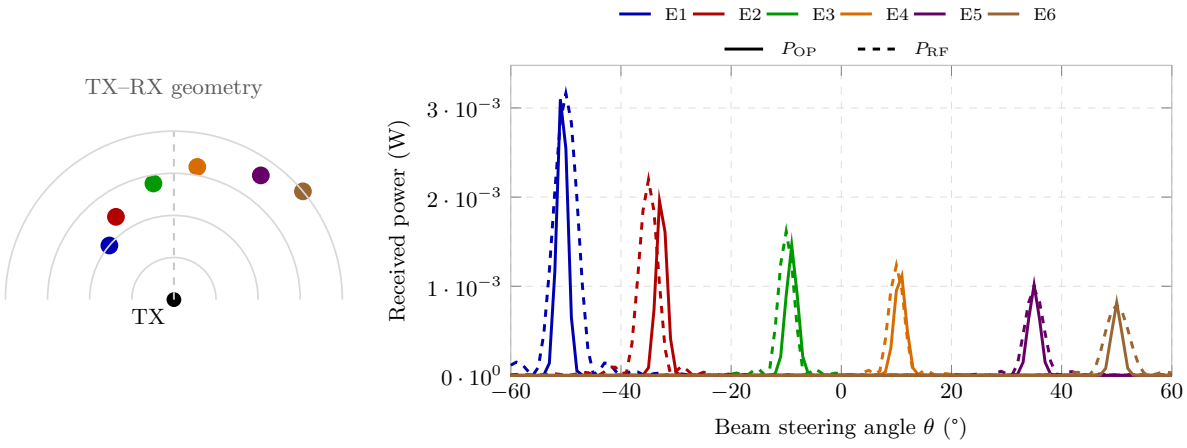


FIGURA 6. Comparison of the equivalent optical and RF received-power responses. Each color identifies one experimental condition, whereas the solid and dashed line styles represent the equivalent optical response P_{OP} and the RF beamforming response P_{RF}, respectively. The six conditions cover TX–RX distances from 1,0 to 2,0 m and receiver angular positions from $-50°$ to $50°$.

dex.html.

CONCLUSION

This work presented an optical experimental approach for emulating selected observable characteristics of the directional behavior of an RF beam generated through beamforming, with particular interest in wireless energy harvesting and energy management applications. Rather than reproducing the electromagnetic behavior or energy-transfer mechanisms of the RF system, the proposed approach uses a directional optical beam and an optical receiver to represent the equivalent power available under different spatial and angular conditions. The empirical RF–optical correspondence yielded $\hat{\alpha} = 8{,}0978 \times 10^{-15}$ and $\hat{\beta} = 3{,}6559$, with a regression slope of $0{,}9878$ and $R^2 = 0{,}9986$, indicating a strong correspondence between the equivalent optical and RF power.

Experimental validation across six receiver positions showed that the optical system approximates both the angular position and the magnitude of the main response predicted by the RF reference model, while the most significant systematic discrepancies occur in the beamwidth, particularly in the FWHM. These differences also reflect experimental factors such as background illumination, measurement noise, positioning uncertainty, and angular misalignment. Overall, the results support the proposed optical system as a low-complexity experimental alternative for studying selected directional characteristics of RF beamforming and spatial power availability, particularly for wireless energy harvesting and energy management, within the characteristics that can be represented and validated through the established empirical correspondence. Since no experimental RF array measurements were performed, the reported correspondence is limited to the ideal RF reference model. Effects such as phase errors, antenna coupling, impedance mismatch, and hardware tolerances remain outside the scope of this study.

AUTHOR AND CONTRIBUTOR CONTRIBUTION STATEMENT

Eduardo Gutiérrez: Software, Methodology, Investigation, Validation, Experimentation, Writing – Original Draft. **Carlos Castorena**: Conceptualization, Methodology, Supervision, Project Administration, Writing – Original Draft. **Juan A. de Rus**: Technical support and assistance with the experimental work. **Sandra Roger**: Methodology, Writing – Review and Editing. **Carmen Botella**: Methodology, Supervision, Writing – Review and Editing.

ACKNOWLEDGMENTS

This work was supported by Grants PID2023-148671OB-I00 and PLEC2024-011160, funded by MICIU/AEI/10.13039/501100011033 and by ERDF/EU. This research was also partially funded by the Generalitat Valenciana through the Prometeo project CIPROM/2026/037. The authors also gratefully acknowledge the Programa Interinstitucional para el Fortalecimiento de la Investigación y el Posgrado del

https://doi.org/10.36677/rici.v4i3.29503 ISSN: 2992-7447 Noviembre 2026 - Febrero 2027 págs. 89- 105

Pacífico for its support through the Verano de la Investigación Científica y Tecnológica del Pacífico.

Referencias

[1] V. Venkateswaran and A.-J. van der Veen, "Analog beamforming in mimo communications with phase shift networks and online channel estimation," *IEEE Transactions on Signal Processing*, vol. 58, no. 8, pp. 4131–4143, 2010. DOI: 10.1109/TSP.2010.2048321

[2] G. K. J. Fischer, T. Schaechtle, A. Gabbrielli, J. Bordoy, I. Häring, F. Höflinger, and S. J. Rupitsch, "A systematic survey and comparative analysis of angular-based indoor localization and positioning technologies," *IEEE Communications Surveys & Tutorials*, vol. 28, pp. 3830–3869, 2026. DOI: 10.1109/COMST.2025.3567765

[3] M. Kaczyński, Z. Piotrowski, and D. Pietrow, "A survey of machine learning techniques for signal source localization and emitter tracking," *IEEE Access*, vol. 13, pp. 198 390–198 409, 2025. DOI: 10.1109/ACCESS.2025.3629818

[4] W. Ma, L. Zhu, Y. Tan, B. Zheng, Y. Zhang, Y. Zhang, K. Ying, Z. Gao, H. Sun, X. Shao, Z. Xiao, D. Niyato, and R. Zhang, "A survey on reconfigurable and movable antennas for wireless communications and sensing," *IEEE Communications Surveys & Tutorials*, vol. 28, pp. 4842–4882, 2026. DOI: 10.1109/COMST.2026.3663021

[5] S. Claessens, K. Hammoud, P. Dhull, D. Schreurs, and S. Pollin, "Energy and pilot efficient beamforming for los wireless power transfer," *IEEE Transactions on Green Communications and Networking*, vol. 10, pp. 1293–1307, 2026. DOI: 10.1109/TGCN.2025.3623642

[6] F. Silva, P. Pinho, and N. B. Carvalho, "Multibeam beamforming technology in microwave power transfer and harvesting," *IEEE Journal of Microwaves*, vol. 5, no. 4, pp. 918–938, 2025. DOI: 10.1109/JMW.2025.3575342

[7] O. Martínez Rosabal, O. L. Alcaraz López, V. Dala Pegorara Souto, R. Demo Souza, S. Montejo-Sánchez, R. Schober, and H. Alves, "Wireless energy transfer beamforming optimization for intelligent transmitting surface," *IEEE Transactions on Wireless Communications*, vol. 25, pp. 6332–6346, 2026. DOI: 10.1109/TWC.2025.3624479

[8] S. N. Arinze, E. R. Obi, S. H. Ebenuwa, and A. O. Nwajana, "Rf energy-harvesting techniques: Applications, recent developments, challenges, and future opportunities," *Telecom*, vol. 6, no. 3, 2025. DOI: 10.3390/telecom6030045

[9] M. Rybakowski, K. Bechta, C. Grangeat, and P. Kabacik, "Impact of beamforming algorithms on the actual rf emf exposure from massive mimo base stations," *IEEE Access*, vol. 11, pp. 141 956–141 964, 2023. DOI: 10.1109/ACCESS.2023.3341623

[10] J. Hoydis, S. Cammerer, F. Ait Aoudia, M. Nimier-David, L. Maggi, G. Marcus, A. Vem, and A. Keller, "Sionna," 2022, https://nvlabs.github.io/sionna/.

[11] S.-P. Chen and H. Schmiedel, *RF Antenna Beam Forming*. Springer, 2023.

[12] M. Ahn, I. Park, I. Sohn, O.-S. Shin, and H. Ku, "Implementation of digital beamforming system for microwave power transfer with real-time beam scanning," *IEEE Access*, vol. 11, pp. 27 280–27 289, 2023. DOI: 10.1109/ACCESS.2023.3253205

[13] N. R. Dusari, Shipra, and M. Rawat, "Digital beamforming with digital predistortion using xilinx rf soc zcu216," in *2022 IEEE International Conference on Signal Processing and Communications (SPCOM)*, 2022, pp. 1–5. DOI: 10.1109/SPCOM55316.2022.9840819

[14] N.-L. Nguyen, K.-H. Nguyen, J. Nadeem, and J. Ha, "Dynamic beam steering for wireless optical power transfer in iot applications," *Optics Letters*, vol. 49, no. 8, pp. 2025–2028, 2024. DOI: 10.1364/OL.518243

[15] T. Moriyama *et al.*, "Beam shape control system with cylindrical lens optics for optical wireless power transmission," *Energies*, vol. 18, no. 9, p. 2310, 2025. DOI: 10.3390/en18092310

[16] W. Li, Q. Yu, J. H. Qiu *et al.*, "Intelligent wireless power transfer via a 2-bit compact reconfigurable transmissive-metasurface-based router," *Nature Communications*, vol. 15, p. 2807, 2024. DOI: 10.1038/s41467-024-46984-4

[17] D. Lloria, S. Roger, C. Botella-Mascarell, and M. Cobos, "Deep-learning-based aoa and aod estimation in analog millimeter wave mimo systems," *IEEE Transactions on Vehicular Technology*, vol. 75, no. 6, pp. 10 200–10 210, 2026. DOI: 10.1109/TVT.2025.3637908

[18] H. T. Friis, "A note on a simple transmission formula," *Proceedings of the IRE*, vol. 34, no. 5, pp. 254–256, May 1946. DOI: 10.1109/JRPROC.1946.234568